ORIENTAL JOURNAL OF CHEMISTRY
An International Open Access, Peer Reviewed Research Journal
www.orientjchem.org
ISSN: 0970-020 X
CODEN: OJCHEG
2026, Vol. 42, No.(4):
Pg. 1340-1355

Apatite-Based Materials for Heavy Metal Removal: Synthesis Methods, Adsorption Mechanisms, and Environmental Applications: A Review

IMANE EL QOR*, FATNA EDDAQAQ, BAHIJA MOUNIR* and FATHALLAAH BAZI

Laboratory of Analytical and Molecular Chemistry, Faculty of Sciences
Ben M'Sick, Hassan II University of Casablanca,20450, Morocco.
*Corresponding authors E-mail: ielqor@gmail.com, mounir.bahija16@gmail.com

http://dx.doi.org/10.13005/ojc/420409

(Received: May 30, 2026; Accepted: July 25, 2026)

ABSTRACT

The increasing prevalence of heavy metals in industrial effluents is a point of great interest due to their toxicity, persistence, and bioaccumulation. Among all treatment methods, adsorption is noteworthy as it is economical, simple, and eco-friendly. In this review, the application of apatite and apatite-based composites as high-capacity adsorbents for heavy metal removal from aqueous solution is discussed. Various synthesis routes as precipitation, hydrothermal, solid-state, ultrasound-microwave, and sonochemical methods are discussed, highlighting their effects on the structural, morphological, and adsorptive properties of apatites. Surface-modified apatites possess outstanding metal adsorption activity for Pb(II), Cd(II), Cu(II), and Cr(VI) through mechanisms by ion exchange, surface complexation, and precipitation. The findings confirm apatite's huge potential as an environmentally friendly approach for heavy metal remediation.

Keywords: Apatites, synthesis, heavy metals, adsorption, wastewater.

INTRODUCTION

Rapid industrial development in various sectors such as textiles, metallurgy, printing, electroplating, battery manufacturing, among others is generating pollutants such as heavy metals, dyes, pesticides, pharmaceuticals, which contribute to the contamination of wastewater. Among these pollutants, heavy metals such as lead, cadmium, zinc, and chromium represent a major threat to human health and the ecosystem[1], due to their resistance to biodegradation processes, high toxicity, and their accumulation in the environment.

Heavy metals cause a variety of health problems in humans, including lung cancer,

neurological damage, kidney, and cardiovascular diseases, male infertility, insomnia, and other disorders 3. Several sophisticated techniques have been developed to treat wastewater laden with heavy metals, including coagulation-flocculation[4], membrane filtration 5, flotation 6, ion exchange[7], and adsorption 8. The most widely used method among these is adsorption, thanks to its cost-effectiveness, environmental friendliness, ease of application, and high-performance approach[9].

The choice of adsorbent influences the success of the adsorption method. These adsorbents include activated carbon, clays, polymers, carbon nanotubes, and apatites[10]. The characteristics of apatites, such as stability, ecological nature, and the ability of controlling the physical and chemical properties that influence porosity, specific surface area, etc., give these materials significant potential for the removal of heavy metals 11the relationship between the structural parameters of HA and its adsorption characteristics (capacity, selectivity, kinetic parameters.

Apatites constitute a large family of calcium phosphates characterized by a crystalline structure capable of allowing multiple ionic substitutions, giving them a high capacity for immobilizing heavy metals. The most studied apatite is hydroxyapatite, but fluoroapatite, chloroapatite, and modified apatites have also shown good results in metal ion adsorption. Their performance is based on mechanisms of ion exchange, complexation, and precipitation[12–14]. A variety of apatite materials show good adsorption capacity for metal ions such as Pb(II), Cu(II), Zn(II), Ni(II), Cr(VI), and As(V), while remaining stable and environmentally friendly[15,16].

The limitations of pure apatites are their relatively low specific surface area, difficult recovery, potential for agglomeration and low mechanical strength, which limit the large-scale use of pure apatites 13recognized by its peculiar crystal architecture and distinctive attributes showcased the underlying potential in adsorbing heavy metal ions (HMI. To overcome these limitations, several studies have sought to create apatite-based composites with materials such as, clays, biochars, biopolymers, carbonaceous materials, and magnetic materials. These composites have a higher adsorption capacity for heavy metals, easier separation, and improved structural and adsorption properties[16,17].

Recent advances show that apatites and their composites constitute a new generation of adsorbents suitable for the treatment of water loaded with heavy metals thanks to their low cost, their ecological nature, their surface properties and their excellent efficiency[17,18].

This review article begins with an introduction to apatites, including their chemical formula, structure, properties, and various types. It then discusses the various methods of synthesizing apatites, including chemical precipitation, sol-gel, solid-state, and sonochemical methods and compares their impacts on the morphology, structure, and porosity of apatites, which influences their adsorption capacity. Finally, recent experimental results that focus on the removal of heavy metals, such as cadmium, zinc, and lead, by apatites and their composites are discussed, along with the perspectives for future work to improve and enrich the applications of these materials in wastewater treatment.

Apatites

The general formula for apatites is written as: $Me_{10}(XO_4)_6Y_2$. It is an ionic compound consisting of a divalent cation Me such as Ca^{2+}, Sr^{2+}, Ba^{2+} etc, a trivalent anion or a tetravalent anion such as PO_4^{3-} AsO_4^{3-},SiO_4^{4-},GeO_4^{4-} etc., and Y^- which is a monovalent or divalent anion such as F^-, Cl^-, Br^-,HO^- ,O^{2-}etc. Most of these apatite compounds crystallize in the hexagonal system. The structure of apatites is characterized by the possibility of incorporating either cationic or anionic ions [19].

Methods for synthesizing apatites and their composites

Several synthesis methods have been used for apatite production, such as dry methods, wet methods, ultrasonic-microwave methods, and using natural resources or chemical reagents. Each method contains various techniques depending on the experimental conditions and reagents employed, such as the precipitation method [21], the hydrothermal method[22], and the sol-gel method[23], among others[24].

The diversity of apatite preparation

methods influences their structure, shape, specific surface area, porosity, and other physicochemical properties[15]. Figure 2 summarizes the different synthesis techniques discussed in this article.

Wet methods

Precipitation method

This technique is widely used in laboratories because it is simple to use and allows the control of the structure and composition of synthesized apatites [26]. Some relevant studies are described below. A simplified model of the precipitation process for the synthesis of Hap is illustrated in Figure 3.

Thi *et al.* (2024) examined the adsorption and desorption of zinc ions on hydroxyapatite synthesized by the chemical precipitation method using $Ca(NO_3)_2$ and $(NH_4)H_2PO_4$. The pH is maintained between 10 and 12 by adding NH_3 under stirring for 2 hours, followed by aging for 15 hours, then washing. The product was dried at 80°C for 24 hours and finally ground to obtain a white powder. The resulting Hap was characterized using several techniques X-ray diffraction (XRD), Brunauer–Emmett–Teller surface area analysis (BET), Fourier transform infrared spectroscopy (FT-IR) and Scanning electron microscopy coupled with energy dispersive X-ray spectroscopy (SEM-EDS). Results show that the Hap has a specific surface area of 91.42 m²/g. SEM images reveal that it has a rod-like morphology (figure 4), while XRD confirms the crystalline structure without the existence of secondary phases. FT-IR confirms the presence of and characteristic groups of the Hap and pH at the point of zero charge (pHPZC) is determined at 7.34 [27].

After the zinc adsorption process, they regenerated the Hap using an electrochemical desorption process in a deep eutectic solvent of the reline type. Following electrolysis, the regenerated material was characterized a second time using the various analytical techniques employed previously. This characterization demonstrated that the material retained a rod shape similar to that of the initial Hap (Figure 5). In addition, FT-IR spectra and XRD diffractograms, which did not reveal significant changes compared to those observed for the initial material (Figure 5). No secondary phases were detected, and the presence of the and bands was confirmed. After the electrochemical desorption process, the authors reused the regenerated Hap. The tests showed an adsorption capacity of 14.38 mg/g with a removal efficiency of 86.28% after the first cycle. This allows its use in successive adsorption cycles [27].

In another study, Chen et al. (2024) synthesized three types of synthetic apatite -chlorapatite (Clap), hydroxyapatite (Hap), and fluorapatite (Fap) - using the coprecipitation method. Clap was synthesized by titrating a $CaCl_2 \cdot 2H_2O$ solution with a Na_3PO_4 solution under stirring at pH 10, adjusted with ammonia, followed by 24 hours of aging, washing, drying at 60°C, and finally grinding and sieving to obtain Clap powder. Hydroxyapatite was synthesized by the same method, but using $Ca(NO_3)_2 \cdot 4H_2O$ and $(NH_4)_2HPO_4$ as reagents. Fluorapatite was prepared by titration of $(NH_4)_2HPO_4$ and NH_4F in a solution heated to 80°C of $Ca(NO_3)_2 \cdot 4H_2O$, followed by the same steps as above. The three adsorbents are characterized by several analytical techniques (SEM, XRD, EDS, FT-IR,X-ray photoelectron spectroscopy (XPS)). SEM showed that the structure of Hap was flaky. Clap appeared as porous blocks, and Fap formed cubic clusters. Energy dispersive x-ray spectroscopy (EDS) revealed the presence of the chemical elements characteristic of apatites (C, P, O, Ca) as well as chlorine (Cl) for chlorapatite and fluorine (F) for fluorapatite. Characterization also showed that the specific surface area of Hap is greater than that of Clap and Fap, which explains the greater adsorption capacity of Hap for lead ions Pb(II) (1597.16 mg/g) and Cd(II) ions (107.18 mg/g) compared with Fap and Clap[9].

Pawar and Theodore (2024) used the chemical precipitation method to prepare hydroxyapatite from pomegranate peels (Hap-pp). The peels were cleaned, boiled in water, and then filtered. The filtrate obtained was mixed with a solution of calcium nitrate and ammonia and incubated for 1 day. The mixture was then added to a solution of ammonium phosphate mixed with ammonia and left for 10 to 12 days. The precipitate formed was washed after drying at 80°C for 24 hours. The prepared adsorbent was characterized by various methods (XRD, FT-IR, SEM-EDS, and BET). Characterization revealed that the synthesized hydroxyapatite has a flat, porous morphology with a specific surface area of 99.021 m²/g and pore

diameters of 24.608 nm. XRD analysis confirmed the presence of the hydroxyapatite crystalline phase (figure 6), while FT-IR revealed the presence of the characteristic functional groups PO_4^{3-} and OH^- with the PO_4^{3-} existence of the carbonate group resulting from the interaction between hydroxyapatite and CO_2 (figure 7)[28].

After Cr(VI) adsorption, the authors carried out a second characterization of the material and successfully confirmed through this characterization that Hap-pp surface modification had taken place, thus confirming that an interaction exists between chromium ions and the adsorbent material. FT-IR spectra showed the shift of several bands, such as those of the OH^- group and phosphate and carbonates, reflecting the participation of these functional groups in the adsorption process (figure 7). SEM analysis revealed a change in morphology, which was initially flat and porous and became more irregular with the appearance of chromium ion deposits (figure 8). EDS analysis showed that the appearance of chromium was accompanied by a decrease in calcium and phosphorus content, confirming its adsorption (figure 9). They used the material for reuse studies after adsorption, which showed that it remained stable and effective for up to 5 cycles in treating chromium ion- contaminated water [28].

In addition, Ahmed Saud Abdulhameed and colleagues prepared a composite based on chitosan, vanillin, and hydroxyapatite for efficient removal of the brilliant green dye. The composite was synthesized by dissolving hydroxyapatite and chitosan in acetic acid under stirring for 24 hours. The mixture was then introduced dropwise into a NaOH solution to form chitosan/hydroxyapatite beads. The beads were washed and then chemically treated by incubating them in a vanillin solution at 40 °C for 2 hours. After rinsing, the resulting beads were dried and then ground. Characterization of this composite showed the presence of a mesoporous structure with a specific surface area of 18.49 m²/g and a pore diameter of 4.31 nm[29].

Wenbin Zhou et al. (2023) developed a composite of carbon nanotubes and iron-doped hydroxyapatite through a multi-step synthesis starting with the sonication of the carbon nanotubes

Table 1: Characteristics of synthesis techniques

Synthesis Method	Advantages	Disadvantages	References
Precipitation	Low cost, use of simple equipment, easy to handle, control of reaction parameters (pH and temperature).	Generally low crystallinity, presence of impurities, slow reaction, need to control reaction parameters.	15,50–53
Hydrothermal	High crystallinity, less agglomeration, high purity.	Higher cost, special, more complex equipment, high temperature and pressure required.	54–57
Sol-Gel	High purity, well-defined morphology.	High cost, time consuming, complex process.	25,58–61
Microwave-Ultrasonic	High purity, simple process, environmentally friendly.	Specific equipment is required.	15,24,62
Sonochemical	Less agglomeration, particles have a uniform size, speed of the process.	Limitation in morphology control	45,47,63,64
Solid state	Simplicity, high crystallinity.	Requires a very high temperature, the shape of the particles is irregular.	65–68

Table 2: The efficacy of apatite-based adsorbents in extracting heavy metals from aqueous solutions

Adsorbents	Heavy metals	Time (min)	Temperature (°C)	pH	Adsorbent dosage (g/L)	Initial conc. (mg/L)	Maximum adsorption capacity (mg/g)	Isotherm model	Kinetic model	Ref.
Hydroxyapatite/ /activated carbon (HAP/AC)	Cu	1440	50	5	1 g/L	300	299.05	Freundlich	Pseudo-second ordre	79
Chitosan/Fluorapatite (CS-Fa)	Cr	36.63	5.75	2.54	86.72mg	100	100.92	Langmuir	Pseudo-first ordre	80
KOH-Modified Hydroxyapatite	Pb	10	-	4	-	-	43.86	Langmuir	-	81
Nanochitosan/sodium alginate/CMC/ HAP	Cu	300	-	6	0,5g	50	512.79	Freundlich	Pseudo-second ordre	82
Zinc phosphate/ hydroxyapatite nano-rods core/shell (ZPh/HPANRs)	Co, Ni	1440	30	7	0,25 g/L	0.25	758 (Co),515.4(Ni)	Langmuir	Pseudo-second order (Co) Pseudo-first order (Ni)	83
Shrimp Shell Chitosan / hydroxyapatite	Cd	50	25	6	2 g/L	100	128.65	Freundlich	Pseudo-second order	84
HAp	Zn, Cu	-	21	8	0,1 g/L	-	60.2 (Cu), 37.9 (Zu)	Langmuir	Pseudo-second order	85
chitosan/fluorapatite (Cs-Fap)	Pb	60	-	4	2 g/L	100	60.24	Langmuir	Pseudo-second order	86
Activated Fluorapatite	Cr	40	-	2	10 g/L	2	0,87	Freundlich	-	87

in nitric acid for 20 minutes, followed by washing and drying at 90 °C. The second step concerns the preparation of the composite: they mixed 0.56 g of carbon nanotubes with a solution of Ca□$(NO_3)_2$ containing the iron ions, then added dropwise a solution of $(NH_4)_2$ HPO_4 under stirring while maintaining the pH at 10. The mixture was aged for 24 hours, filtered, rinsed, dried at 90 °C, and finally calcined at 300 °C for 3 hours. Characterization results showed a specific surface area of 255.68 m²/g, an average pore diameter of 9.53 nm, and a mesoporous structure [30].

Another composite is synthesized from activated carbon derived from corncobs and hydroxyapatite extracted from catfish by Setiawan et al. (2024). The was prepared through a multistep process. Activated carbon was synthesized by carbonizing corncobs at 600 °C for 60 min, then activated with phosphoric acid (H_3PO_4) for 24 hours, followed by washing, and drying at 105 °C. Hydroxyapatite was prepared from catfish bones that have been cleaned, treated twice with NaOH at 70 °C under stirring, then filtered and treated with H_3PO) to neutralize the mixture before drying. The activated carbon/hydroxyapatite composite was prepared by mixing the two adsorbents in different proportions, stirred with ethanol, dried, sieved and then calcined at 500 °C for 5 hours to form the composite. The results of the characterization of this composite showed a specific surface area of 419.02 m²/g and the presence of the characteristic groups O-H, P-O, and □CO_3^{2-} [31].

Hydrothermal method

The hydrothermal method is among the common methods used for apatite synthesis. It requires high temperatures and pressures, hence the need for an autoclave or pressure vessel [33]. By modifying experimental conditions (temperature and pressure), apatite properties such as porosity, crystallinity, and morphology can be controlled.

A simplified model of the hydrothermal process for the synthesis of Hap, as illustrated in Figure 10.

Sheng-Yuan Peng and their colleagues used the hydrothermal method to recycle calcium-rich limestone sludge to produce hydroxyapatite. They began by dissolving the limestone sludge in nitric acid NH_3. The calcium-rich filtrate was mixed with in different proportions to adjust the Ca/P molar ratio to 1, 1.67, 2.33, or $(NH_4)_2$ HPO_4, while adjusting the pH to 10 with NaOH. The mixtures were heated in a Teflon autoclave at temperatures ranging from 393 K to 453 K for 8 hours. The precipitates were then washed and dried at 90 °C for 24 hours. FTIR, Transmission Electron Microscopy (TEM), and Nuclear Magnetic Resonance (NMR) then

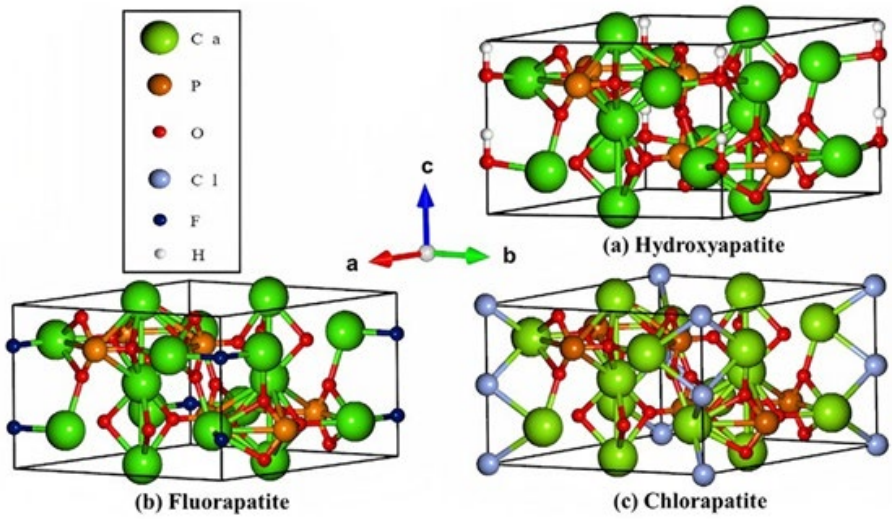

Fig. 1: A schematic illustration of three different types of apatites: (a) Hydroxyapatite (Hap), (b) Fluorapatite (Fap), and (c) Chlorapatite (Clap) 20

characterized the samples obtained. The analyses confirmed the formation of hydroxyapatite with predominantly rod-shaped particle morphology. Hydroxyapatite crystallinity depends on hydrothermal temperature. At 393 K, crystallization is incomplete; at 423 K, structures are well crystallized; at 453 K, crystallinity becomes more pronounced [34].

A similar approach was adopted by Ya-Wen Lin et al. (2024). The synthesis method was based on fine limestone sludge, but this time using cetyltrimethylammonium bromide (CTAB) and 1,3,5-triethylbenzene (TMB) as a pore expander. The preparation involved mixing fine limestone sludge, CTAB, and TMB in deionized water under stirring at pH 10, adjusted with NaOH. Afterwards□$(NH_4)_2$ HPO_4, was gradually added to adjust the Ca/P ratio to 1, followed by hydrothermal treatment at temperatures ranging from 120 °C to 180 °C for 8 hours. The precipitate was centrifuged, washed, dried at 60 °C for 24 hours, and then calcined in an oven at 550 °C for 6 hours. The resulting product was characterized by XRD, SEM, Differential thermal analysis/Thermogravimetric analysis

(DTA/TGA), and BET methods. Characterization results showed that the temperature, the TMB/CTAB ratio, and the use of agents enabled control of the crystallinity, morphology, and porosity of the synthesized adsorbent. The increase in the TMB/CTAB ratio expanded the pore diameter and increased the specific surface area. Similarly, the crystallinity of the material increased with increasing temperature. On the other hand, SEM analysis confirmed the presence of a rod-like morphology with lengths that vary depending on the temperature value [35].

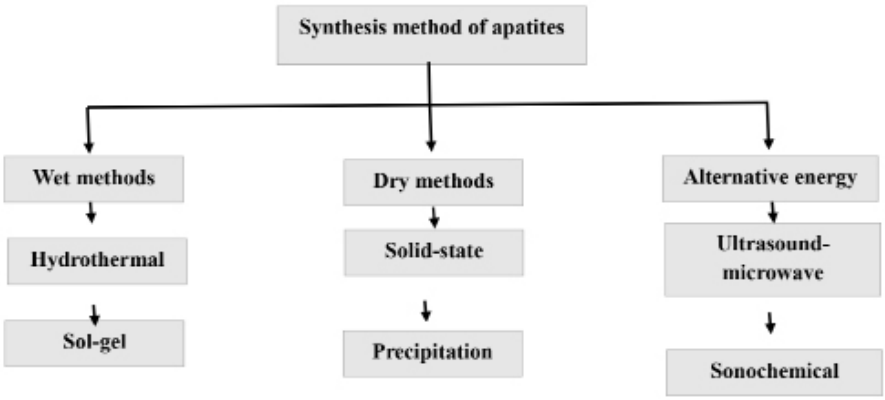

Fig. 2: Synthesis method of apatites [25]

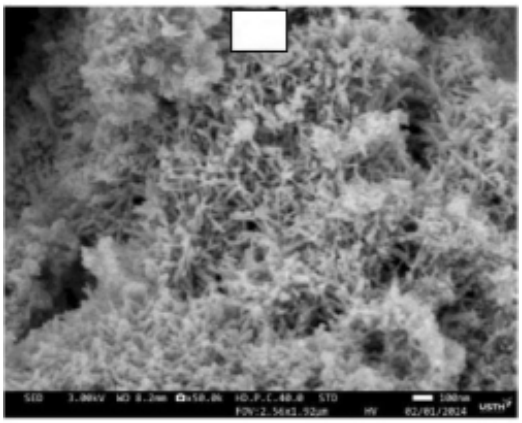

Fig. 3: SEM image of HAp[27]

Sol-gel method

The sol-gel technique is characterized by its control of both the morphology and chemical composition of apatites. The control of the synthesis parameters prevents the formation of secondary phases. This technique involves the use of phosphate and calcium precursors to obtain a colloidal solution that transforms into a gel [36]. A simplified model of the sol-gel method is illustrated in Figure 11.

P. Yasotha and his collaborators prepared TiO_2-doped hydroxyapatite using the sol-gel method. The preparation began with mixing a calcium hydroxide ($Ca(OH)_2$) solution with a phosphoric acid (H_3 PO_4) solution under stirring for 30 min at

pH 10. Then, a titanium isopropoxide solution was added dropwise. Afterwards, the precipitate formed was treated with ultrasound for 30 min, followed by washing, filtration, and drying at 70 °C for 5 hours. Characterization of the nanocomposite (Hap/TiO_2) by XRD shows the presence of a hexagonal structure. XPS confirmed the existence of Ca, P, Ti, and O, while SEM revealed an agglomerated spherical morphology [37].

In another scientific research, a nanocomposite was prepared by Jang et al using hydroxyapatite and graphene oxide. They mixed two solutions, one containing graphene oxide and the other calcium nitrate tetrahydrate at basic pH (pH>10) followed by ultrasonic treatment for 10 min. Then, they added to the mixture a solution of monobasic ammonium phosphate, followed by stirring for 15 hours, centrifugation, washing, and drying at 50 °C. EDS characterization reveals a Ca/P ratio of about (1.60 ± 0.05), close to 1.67, which represents the stoichiometric value of hydroxyapatite. On the other hand, SEM analysis shows the presence of nanoparticles in the form of rod-shaped of a size of 100 nm [38].

Another compound consisting of magnesium-doped hydroxyapatite (MHAP) was synthesized using the sol-gel technique. A solution of calcium nitrate $Ca(NO_3)_2$ was mixed with a solution of magnesium nitrate $Mg(NO_3)_2$ at different Mg/Ca molar ratios. Afterwards, A solution of phosphoric acid H_3PO_4 was added to the first mixture, followed by stirring at 30 °C while pH 10 was adjusted with ammonia. The resulting gel was filtered, washed, dried, and calcined at 300 °C for 2 hours. Characterization of the obtained material revealed that increasing the Mg/Ca molar ratio increased the specific surface area and decreased the particle size and crystallinity [39].

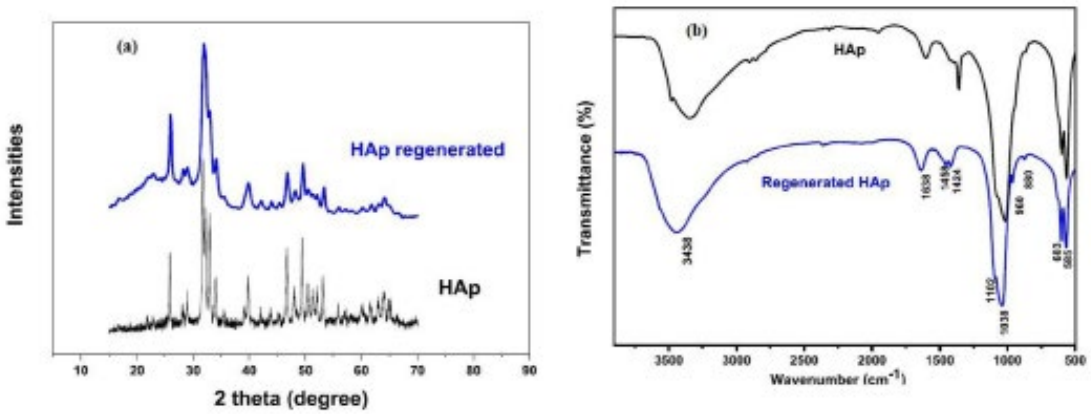

Fig. 4: XRD pattern (a) and FT-IR spectra (b) of original HAp, regenerated Hap[274]

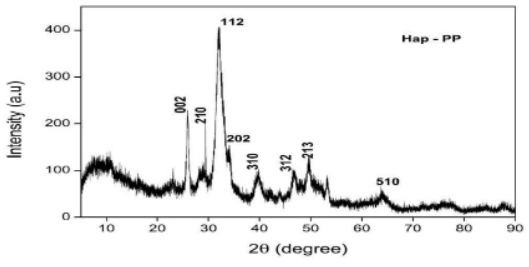

Fig. 5: XRD pattern of Hap-PP [28]

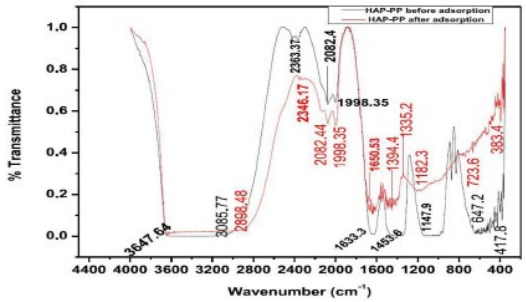

Fig. 6: FTIR spectra of Hap – PP before and after Cr (VI) adsorption[28]

Dry methods

The solid-state method is an easy technique that involves mixing chemical reagents, grinding and calcining them at high temperatures to synthesize the desired apatite [40]. Mobarak et al. (2023) synthesized Hap by calcining a finely ground blend of eggshell powder and diammonium phosphate at 950 °C, following grinding under mechanical ball milling at 450 rpm for 6 hours. The specific surface area of the synthesized material was determined by the BET technique, which revealed a value of 10.11 m²/g with a pore diameter of 8.2 nm. On the other hand, Field emission scanning electron microscopy (FESEM) and Transmission electron microscopy (TEM) confirmed the presence of the particles in spherical and plate form. The obtained adsorbent demonstrated effective removal of Congo Red dye with a maximum adsorption capacity of 9.64 mg/g [41].

Mobarak et al. (2022) also, in another article, compared the photocatalytic behavior of HAp synthesized by solid-state (S-HAp) and wet chemical precipitation (W-HAp) synthesis methods. The S-HAp, synthesized by calcination at 900 °C after intensive grinding, possessed a biphasic composition (high β-Tricalcium Phosphate (β β-TCP)) and reduced crystallinity, which benefited reactive species formation. These findings confirm the viability of the solid-state process as a green route for biomass waste valorization and the production of high-performance as a photocatalyst for the degradation of dyes [42]. A simplified model of the solid-state process for the synthesis of Hap, as illustrated in Figure 12.

Alternative energy methods

Ultrasound-microwave method

The synthesis of nanostructured hydroxyapatite (nano-HAp) using the ultrasound-microwave method combines the advantages of microwave heating and ultrasonic irradiation to prepare highly crystalline materials with controlled morphology. In the study by Poinern et al. (2009), Nano-HAp was synthesized by chemical precipitation under ultrasonic irradiation (0 W, 25 W and 50 W, 30 kHz) from $Ca(NO_3)_2$ and KH_2PO_4 solutions at a fixed Ca/P ratio of 1.67 and a pH of 9. The resulting spherical particles (30nm) were then thermally treated, which enhanced their crystallinity and

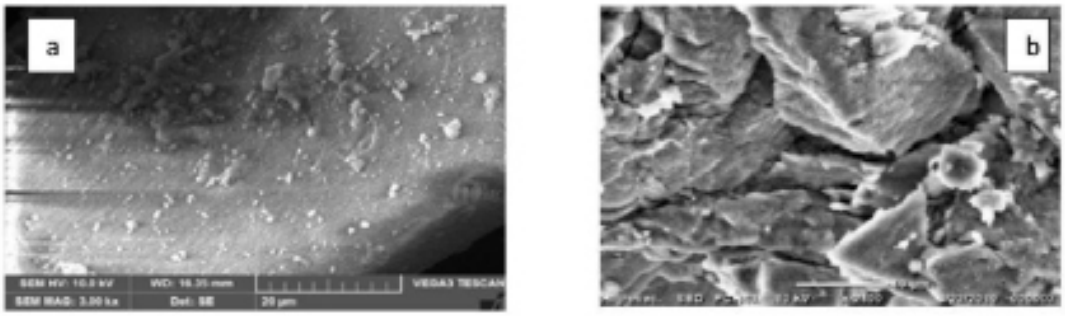

Fig. 7: SEM images of Hap – PP [28]

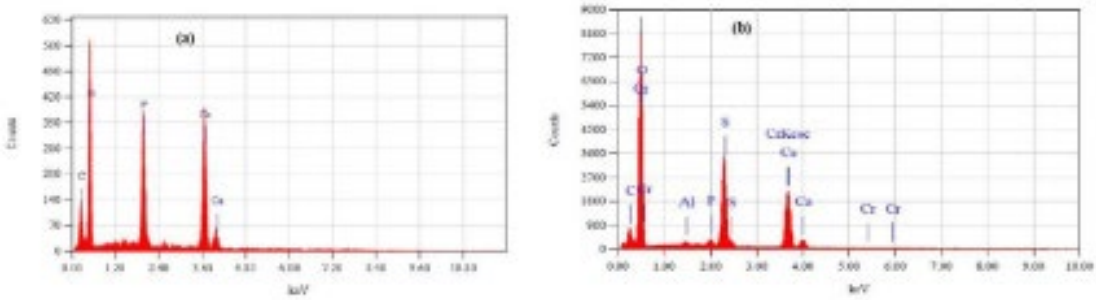

Fig. 8: EDS images of Hap - PP (a) before, and (b) after adsorption[28]

reduced agglomeration [43]. The same technique was employed by Putro et al. (2014) to convert Pomacea sp shells to nano-HAp, where particles were dispersed via ultrasonication and microwaves were used to accelerate the reaction to yield mixed-phase crystals (HAp, CaO, □Ca(OH)$_2$) of 0.46-2.5 μm size [44].

Sonochemical method

The sonochemical method has been very effective for the preparation of nanostructured hydroxyapatite (HAp) adsorbents from various biota sources. Edralin et al. (2017) prepared HAp nano-rods from mussel shells using a sonochemical method, achieving uniform rod-shaped structures (30–80 nm in length) with high photocatalytic activity (86.8% degradation of Rhodamine B). XRD characterization confirmed the hexagonal phase of HAp and FTIR identified phosphate and carbonate groups, indicating structural integrity [45].

Utara and Klinkaewnarong (2015) synthesized a hydroxyapatite from natural rubber latex. TEM analysis revealed the presence of nano-rod particles, and XRD analysis showed the presence of two phases: one corresponding to Hap and the other to ββ-TCP [46]. On the other hand, Ferrairo et al. (2023) prepared a hydroxyapatite from bovine bones, using two methods: the sonochemical method and the mechanochemical methods, to make a comparison between them. Both techniques showed a conservation of the crystalline structure of Hap, while the particles prepared by the sonochemical method were larger than those prepared by the mechanochemical method, 60 nm and 40 nm, respectively [47].

In addition to the use of apatites synthesized by the sonochemical method in adsorption, they are also used to prepare apatite-based materials for medical applications and in catalysis.

In another study, Ekka et al. (2018) developed a photocatalyst based on hydroxyapatite

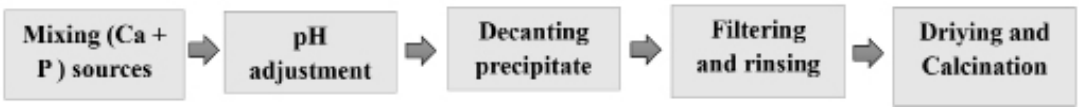

Fig. 9: Preparation of HAp using the precipitation method 32

Fig. 10: The hydrothermal method for preparing a hap[32]

Fig. 11: The Sol-gel method for preparing a hap[32]

Fig. 12: Preparation of HAp by the solid-state method [32]

and zirconium dioxide ZrO_2 by the sonication method for 4 hours. The obtained material gave good results for the degradation of phenols (>95 %). Characterization revealed a uniform dispersion of ZrO_2 nanoparticles (10±5 nm) on HAp.

These studies demonstrate that sonochemical method allows for control over surface properties, nanocomposite morphology, and specific surface area with enhancement in their performance for intended applications [48]. A simplified model of the sonochimical process for the synthesis of Hap, is illustrated in Figure 13.

Comparison of the techniques used for synthesis

Various methods of apatite synthesis are used in the literature, each with its own advantages and disadvantages, as shown in Table 1. Selection of the method to be used for synthesis depends on a number of factors, such as available resources, the desired purity, process complexity, and cost[49].

Wet methods such as precipitation and sol-gel are commonly used for apatite synthesis, due to their simplicity and low cost. However, these techniques require strict control of reaction parameters (pH, temperature, etc.), which influence reaction time. On the other hand, dry methods such as the solid-state method do not require the use of solvents, but they do need high temperatures and thus yield products of reliable quality[50]. In parallel, sonochemical synthesis produces uniform products with less agglomeration, even if its energy yield is sometimes limited. Finally, the microwave-ultrasonic technique is fast and offers good yield, but requires specific equipment[24].

A detailed comparison of the advantages and disadvantages of these methods is presented in Table 1.

Adsorption removal of heavy metals by apatite and its composites

The treatment of wastewater contaminated with heavy metals has been a subject of research in many recent studies. Chen et al. (2024) studied and compared the absorption capacity of three types of apatites (hydroxyapatite (Hap), chlorapatite (Clap), and fluorapatite (Fap)) for the removal of Pb(II) and Cd(II). They prepared the three forms of apatites using the coprecipitation method. The maximum absorption capacities for Pb(II) were 1597.16 mg/g (Hap), 1477.82 mg/g (Clap), and 1455.99 mg/g (Fap), and for Cd(II) were 107.18 mg/g (Hap), 79.08 mg/g (Clap), and 15.8 mg/g (Fap). The absorption efficiency depended on the pH value: lead adsorption was highest at pH 3, while cadmium adsorption was highest at pH 4. The mechanisms involved in

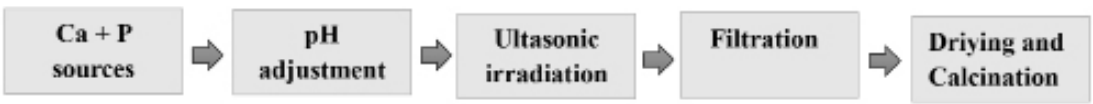

Fig. 13: Preparation of HAp by the sonochimical method[32]

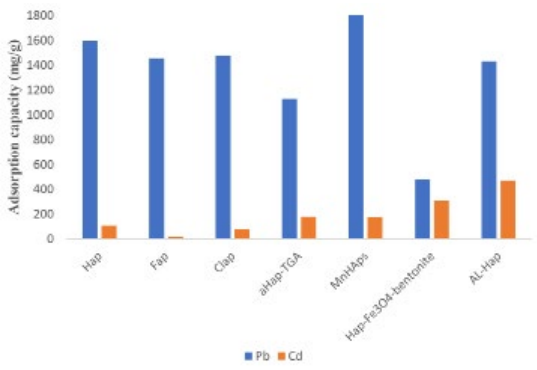

Fig. 14: Comparison of the adsorbent capacity of several apatite-based materials

the absorption of the two metals included surface complexation, ion exchange, electrostatic attraction, and dissolution-precipitation. The latter is dominant for Pb(II), as demonstrated by equations (1) and (2)[9]which requires urgently seeking an efficient and cost-effective solution. Apatite as the most abundant phosphate on earth exhibits remarkable adsorption effect on heavy metals. Based on this, three kinds of apatite adsorbents were prepared in this study by titration co-precipitation method for the removal of heavy metals Pb (II :

$$Ca_{10}(PO_4)_6(OH,Cl,F)_2 + 14H^+ = 10Ca^{2+} + 6H_2PO_4 + 2(H_2O, HCl, HF) \quad ...(1)$$

$10\ Pb\square_2^{2+} + \square 6H_2PO_4 + \square 2\ (H_2O, HCl, HF) = Pb_{10}(PO^4)_6(OH,Cl,F)_2 + 14\ H^+$ ...(2)

For their part, Chowdhury et al. (2025) prepared a nanocomposite combining hydroxyapatite, aluminum, and thioglycolate (aHap-TGA) with a polyacrylonitrile matrix. The adsorption capacities of this nanocomposite are remarkable, reaching 1131 mg/g for Pb(II) and 177 mg/g for Cd(II). The absorption mechanism was described by the Langmuir isotherm and the pseudo-second-order model, confirming chemisorption[69].

Butrin et al. (2024) prepared a composite consisting of activated carbon and hydroxyapatite (HAP/AC) to remove Cu(II) copper ions. They used the one-pot technique to prepare this material. The results revealed an adsorption capacity of 299.05 mg/g at pH 5 and 50 °C. The adsorption isotherm followed the Freundlich model, while the kinetics followed the pseudo-second-order model. The main mechanisms involved were complexation, cation exchange, and electrostatic interaction 70, as indicated by the following equations (3) and (4) :

$= POH + Cu^2 + = \square\square POCu^+ + H^+$ ....(3)

$Ca_{10}\square(PO_4)_6(OH)_2 + xCu^{2+} = Ca_{10-x}Cu_x\square(PO_4)_6(OH)_2 + xCu^{2+}$ ...(4)

In another study, Yuan et al. (2023) presented a significant improvement in Cd(II) adsorption, reaching 60.7 mg/g by using biochar derived from rice husks and wheat straw modified with nano-chlorapatite. The optimal pH ranged from 6 to 8. The Langmuir isotherm model and pseudo-second-order kinetics best describe the adsorption mechanism, suggesting chemisorption dominated by precipitation, surface complexation, and ion exchange [71].

On the other hand, Chen et al. (2025) synthesized composites of hydrochar derived from photoremediated biomass and hydroxyapatite-rich bone meal. The maximum adsorption capacity of these materials reached 42.08 mg/g for Cd(II) and 29.44 mg/g for Zn(II), at pH 6.0 and 298.15 K temperature. The absorption mechanism of Zn(II) was better described by the Langmuir isotherm; whereas Cd(II) adsorption followed the Freundlich model. Electrostatic interactions, ion exchange, precipitation and complexation, and cation-π interactions represent the adsorption mechanisms of both metals [72].

Similarly, Rout et al. (2024) developed alginate beads containing a nanocomposite of activated carbon coated with silver-doped hydroxyapatite. This material demonstrated a high removal rate for the three pollutants studied: 95% for Pb(II) and U, and 85% for Cd(II). The adsorption kinetics followed the pseudo-second-order model, and chemisorption is the adsorption mechanism involved in the removal of these pollutants[73].

Han et al. (2020) used eggshells to prepare a chlorapatite for use in removing chromium Cr(VI) ions. The adsorption mechanism followed the Langmuir isotherm with a maximum adsorption capacity of 63.47 mg/g at pH 3 and pseudo-second-order kinetics. The adsorption process of chromium ions was dominated by chemisorption[74].

On the other hand, to remove zinc, copper, and cobalt, Abukhadra et al. (2018) synthesized a Ni/Fe doped carbonate fluorapatite. The adsorption test results revealed capacity values reaching 149.25 mg/g, 147.05 mg/g, and 106.4 mg/g for Zn^{2+}, Cu^{2+}, and Co^{2+}, respectively. The adsorption isotherm and kinetics followed the Langmuir and pseudo-second-order models with a mechanism governed by ion exchange and precipitation75. Table 2 summarizes the adsorption efficiency of apatite-based adsorbents in heavy metal removal.

This review demonstrates the capacity of apatites and their composites for heavy metal removal. The adsorption mechanism is generally heterogeneous and governed by the pseudo-second-order model [24].

Figure 14 shows the adsorption capacities of some apatite-based materials for the removal of lead and cadmium. The graph shows that the adsorption capacity of lead by the different materials used is greater than the adsorption capacity of cadmium. Moreover, the removal rate of these two metals varies from one adsorbent to another, which shows that the removal capacity depends on both the nature of the adsorbent and the adsorbate used. For example, the three apatites (Hap, Fap and Clap) represent a significant adsorption capacity for the lead ion Pb(II) of 1597.16 mg/g, 1477.82 mg/g and

1455.99 mg/g for Hap, Clap and Fap respectively, while notably low values for the cadmium ions Cd(II) of 107.18 mg/g, 79.08 mg/g and 15.8 mg/g for Hap, Clap and Fap respectively[9].

Unlike the two hydroxyapatite-based compounds, Mn-HAp (doped with manganese) and AL-HAp (with alendronate), the doping effect gave more favorable capacity values for both metals. MnHaps material exhibits an adsorption capacity of 1806.09 mg/g for Pb(II) and 176.88 mg/g for Cd(II) [76,77]. Similarly, AL-Hap reaches 1431.8 mg/g and 469 mg/g for Pb(II) and Cd(II), respectively [76].

On the other hand, apatite-based composites such as HAp-Fe_3O_4-bentonite and aHap-TGA also show notable values in the removal of these two pollutants. The HAp-Fe_3O_4-bentonite composite shows a notable capacity of 309 mg/g for Cd(II) 78. On the other hand, the aHap-TGA nanocomposite achieves capacities of 1131 mg/g for Pb(II) and 177 mg/g for Cd(II) due to the addition of the sulfonate functional group[69].

Finally, the modification of the physicochemical properties of apatites, either through doping or by preparing composites with other materials, promotes the elimination of heavy metals from wastewater.

Perspectives

The treatment of water loaded with heavy metals using synthetic apatites and their composites has given favorable results in several studies. However, further research is still required to address existing limitations met by other researchers to improve their use and efficiency:

1. Hydroxyapatite is one of the most widely used apatites by researchers due to its high specific surface area, durability, and low toxicity[88]. However, it suffers from limitations related to its fragility, surface nature, and porosity[89]. In order to overcome these limitations, researchers have prepared apatite-based materials; yet, these materials also have disadvantages such as high cost and limited applicability on an open scale and in real conditions. Therefore, as a perspective for future work, it is necessary to focus on the synthesis of a low-cost apatite-based material with notable performances in real environments and on a large scale[13].
2. Generally, studies carried out with apatite-based adsorbents have been conducted at the laboratory scale, therefore, tests with these compounds must be carried out on an industrial scale[90].
3. The use of natural apatitic materials has been the subject of several scientific researches without testing the toxicity of these materials towards humans and the ecosystem.
4. Finally, future research should focus on the development of new theoretical models to better explain and understand the complex adsorption mechanisms of these new synthesized materials[13].

CONCLUSION

Heavy metals, pesticides, dyes, pharmaceuticals, and other substances are pollutants that pose a significant risk to human health and the ecosystem. To address wastewater pollution caused by these pollutants, several adsorbents have been used. Among these, apatites and their composites have demonstrated remarkable adsorption capacity in removing these pollutants, particularly heavy metals.

In this review, we studied various routes of synthesis of apatites and apatite composites like precipitation, hydrothermal, sol-gel, sonochemical, and microwave/ultrasound methods. Each of these methods has its own advantages and disadvantages and affects the structural, morphological, and surface properties of the resulting materials differently, which influences their adsorption capacity. On the other hand, apatite-based compounds have demonstrated a high adsorption capacity for various metal ions, according to different mechanisms such as precipitation, complexation, ion exchange, and electrostatic interactions. Despite these promising results, the article identified some of the constraints and research needs to guide future research into these materials.

ACKNOWLEDGEMENT

The authors thank Université Hassan II de Casablanca, Faculty of Sciences Ben M'Sik, and the Laboratory of Analytical and Molecular Chemistry for their scientific support, technical assistance, and

research facilities during this work.

Conflict of Interest

The author(s) do not have any conflict of interest.

Funding Source Statement

This research was supported by Hassan II University of Casablanca, Morocco.

Authors' Contributions

Imane El Qor

Conceptualization, data collection, manuscript writing and editing.

Bahija Mounir

Supervision, critical review, and manuscript revision. All authors have read and approved the final version of the manuscript.

Data Availability Statement

This statement does not apply to this article.

Ethical Approval Statement

This statement does not apply to this article.

Informed Consent Statement

This study did not involve human participants, and therefore, informed consent was not required.

REFERENCES

1. Mobasherpour, I.; Salahi, E.; Pazouki, M. *Arab. J. Chem.* **2012**, *5* (4), 439–446.
2. He, M.; Zhang, Z.; Wang, M.; Liang, C.; Wang, H.; Cheng, C.; Li, Y.; Wang, Y.; Zhang, Z. *J. Hazard. Mater.* **2025**, *481*, 136525.
3. Ayodele, O.; Olusegun, S. J.; Oluwasina, O. O.; Okoronkwo, E. A.; Olanipekun, E. O.; Mohallem, N. D. S.; Guimarães, W. G.; Gomes, B. L. F. D. M.; Souza, G. D. O.; Duarte, H. A. *Environ. Nanotechnol. Monit. Manag.* **2021**, *15*, 100439.
4. Skotta, A.; Jmiai, A.; Elhayaoui, W.; El-Asri, A.; Tamimi, M.; Assabbane, A.; El Issami, S. *J. Taiwan Inst. Chem. Eng.* **2023**, *145*, 104792.
5. Atallah, C.; Mosadeghsedghi, S.; Dashtban Kenari, S. L.; Hudder, M.; Morin, L.; Volchek, K.; Mortazavi, S.; Ben Salah, I. *Desalination Water Treat.* **2024**, *320*, 100730.
6. Benmansour, M. R.; Taakili, R.; Gaysinski, M.; Orange, F.; Makan, M.; Etahiri, A.; Mazouz, H.; Benhida, R. *Miner. Eng.* **2024**, *216*, 108857.
7. Jasim, A. Q.; Ajjam, S. K. *South Afr. J. Chem. Eng.* **2024**, *49*, 43–54.
8. Tank, S.; Pandey, M.; Rath, J. J.; Bandyopadhyay, M. *Hybrid Adv.* **2025**, *10*, 100489.
9. Chen, H.; Xiao, R.; Huang, D.; Deng, R.; Li, R.; Chen, Y.; Zhou, W. *J. Mol. Liq.* **2024**, *400*, 124478.
10. Andrew Ofudje, E.; Sodiya, E. F.; Olanrele, O. S.; Akinwunmi, F. *Heliyon* **2023**, *9* (2), e12971.
11. Ivanets, A. I.; Kitikova, N. V.; Shashkova, I. L.; Roshchina, M. Yu.; Srivastava, V.; Sillanpää, M. *J. Water Process Eng.* **2019**, *32*, 100963.
12. Li, Z.; Qiu, Y.; Zhao, D.; Li, J.; Li, G.; Jia, H.; Du, D.; Dang, Z.; Lu, G.; Li, X.; Yang, C.; Kong, L. *Sci. Total Environ.* **2023**, *904*, 166918.
13. Wang, T.; Cao, W.; Dong, K.; Li, H.; Wang, D.; Xu, Y. *Chemosphere* **2024**, *352*, 141367.
14. Guru, P. S.; Panda, B.; Parida, K. N. *Mater.* **2025**, *9*, 101042.
15. Biedrzycka, A.; Skwarek, E.; Hanna, U. M. *Adv. Colloid Interface Sci.* **2021**, *291*, 102401.
16. Vaishali; Bendi, A.; Singh, S.; Pundeer, R. *Nanotechnol.* **2026**, *9*, 100339.
17. George, G.; Karunanidhi, G. *Results Surf. Interfaces* **2025**, *21*, 100663.
18. Kharissov, B. I.; Kharissova, O. V.; García, T. H.; Dorozhkin, S. V.; Dimas, A. V.; Zorrilla-Siller, J.; Cordero-Segovia, S. In *Handbook of Ecomaterials*; Martínez, L. M. T., Kharissova, O. V., Kharisov, B. I., Eds.; Springer Nature Switzerland: Cham, 2026; pp 1–28.
19. Sboui, N.; Agougui, H.; Jabli, M.; Boughzala, K. *Inorg. Chem. Commun.* **2022**, *142*, 109628.
20. Roy, A.; Kanungo, B.; Patra, P. K.; Bhattacharya, B. *Mater. Today Commun.* **2023**, *35*, 106223.
21. Mobasherpour, I.; Salahi, E.; Pazouki, M. *Arab. J. Chem.* **2012**, *5* (4), 439–446.
22. Joshi, K. J.; Shah, N. M. *Mater. Today Proc.* **2021**, *47*, 505–509.
23. Robles-Águila, M. J.; Reyes-Avendaño, J. A.; Mendoza, M. E. *Ceram. Int.* **2017**, *43* (15), 12705–12709.

24. Amenaghawon, A. N.; Anyalewechi, C. L.; Darmokoesoemo, H.; Kusuma, H. S. *J. Environ. Manage.* **2022**, *302*, 113989.
25. Pai, S.; M Kini, S.; Selvaraj, R.; Pugazhendhi, A. *J. Water Process Eng.* **2020**, *38*, 101574.
26. Mushtaq, A.; Zhao, R.; Luo, D.; Dempsey, E.; Wang, X.; Iqbal, M. Z.; Kong, X. *Mater. Des.* **2021**, *197*, 109269.
27. Thi Duyen, L.; Tien Dung, C.; Thi Mai Thanh, D.; Thu Phuong, N. *Polyhedron* **2024**, *261*, 117126.
28. Pawar, S.; Theodore, T. *Heliyon* **2024**, *10* (18), e37540.
29. Abdulhameed, A. S.; Abdullah, S.; Altamimi, A. A.; Abualhaija, M.; Algburi, S. *Int. J. Biol. Macromol.* **2025**, *310*, 143140.
30. Zhou, W.; Zhou, X.; Song, W.; Wang, C.; Zhang, H.; Huang, X. *J. Environ. Chem. Eng.* **2023**, *11* (6), 111259.
31. Setiawan, A.; Kusumawati, T. A.; Ramadani, T. A.; Wang, Y.-F.; Kusumawardani, A.; Dermawan, D. *Inorg. Chem. Commun.* **2024**, *167*, 112744.
32. Verma, R.; Mishra, S. R.; Gadore, V.; Ahmaruzzaman, Md. *Adv. Colloid Interface Sci.* **2023**, *315*, 102890.
33. Varadavenkatesan, T.; Vinayagam, R.; Pai, S.; Kathirvel, B.; Pugazhendhi, A.; Selvaraj, R. *Prog. Org. Coat.* **2021**, *151*, 106056.
34. Peng, S.-Y.; Lin, Y.-W.; Lin, Y.-Y.; Lin, K.-L. *Inorg. Chem. Commun.* **2024**, *160*, 111943.
35. Lin, Y.-W.; Peng, S.-Y.; Lin, K.-L. *J. Solid State Chem.* **2024**, *339*, 124914.
36. Azis, Y.; Adrian, M.; Alfarisi, C. D.; Khairat; Sri, R. M. *IOP Conf. Ser. Mater. Sci. Eng.* **2018**, *345*, 012040.
37. Yasotha, P.; Kalaiselvi, V.; Blessymol, B.; Vidya, C.; Tamilarasu, S. *J. Indian Chem. Soc.* **2025**, *102* (4), 101603.
38. Jang, J.-H.; Oh, B.; Lee, E.-J. *Ceram. Int.* **2021**, *47* (19), 27677–27684.
39. Zhou, M.; Yan, X.; Zou, H.; Zhao, Y.; Yin, N.; Zhang, C.; Wang, L. *Desalination Water Treat.* **2019**, *171*, 183–195.
40. Cox, S. C.; Walton, R. I.; Mallick, K. K. *Bioinspired Biomim. Nanobiomaterials* **2015**, *4* (1), 37–47.
41. Bin Mobarak, M.; Pinky, N. S.; Chowdhury, F.; Hossain, Md. S.; Mahmud, M.; Quddus, Md. S.; Jahan, S. A.; Ahmed, S. *J. Saudi Chem. Soc.* **2023**, *27* (5), 101690.
42. Bin Mobarak, M.; Hossain, Md. S.; Yeasmin, Z.; Mahmud, M.; Rahman, Md. M.; Sultana, S.; Masum, S. M.; Ahmed, S. *J. Mol. Struct.* **2022**, *1252*, 132142.
43. Poinern, G. E.; Brundavanam, R. K.; Mondinos, N.; Jiang, Z.-T. *Ultrason. Sonochem.* **2009**, *16* (4), 469–474.
44. Putro, J. N.; Handoyo, N.; Kristiani, V.; Soenjaya, S. A.; Ki, O. L.; Soetaredjo, F. E.; Ju, Y.-H.; Ismadji, S. *Ceram. Int.* **2014**, *40* (7), 11453–11456.
45. Edralin, E. J. M.; Garcia, J. L.; Dela Rosa, F. M.; Punzalan, E. R. *Mater. Lett.* **2017**, *196*, 33–36.
46. Utara, S.; Klinkaewnarong, J. *Ceram. Int.* **2015**, *41* (10), 14860–14867.
47. Ferrairo, B. M.; Mosquim, V.; De Azevedo-Silva, L. J.; Pires, L. A.; Souza Padovini, D. S.; Magdalena, A. G.; Fortulan, C. A.; Lisboa-Filho, P. N.; Rubo, J. H.; Sanches Borges, A. F. *Mater. Chem. Phys.* **2023**, *295*, 127046.
48. Ekka, B.; Nayak, S. R.; Achary, L. S. K.; Sarita; Kumar, A.; Mawatwal, S.; Dhiman, R.; Dash, P.; Patel, R. K. *J. Environ. Chem. Eng.* **2018**, *6* (5), 6504–6515.
49. Sadat-Shojai, M.; Khorasani, M.-T.; Dinpanah-Khoshdargi, E.; Jamshidi, A. *Acta Biomater.* **2013**, *9* (8), 7591–7621.
50. Jobisha, J.; Vinisha, V.; Francy, B. R.; Martin Mani, J. A.; Linet, J. M. *Inorg. Chem. Commun.* **2025**, *177*, 114385.
51. Afshar, A.; Ghorbani, M.; Ehsani, N.; Saeri, M. R.; Sorrell, C. C. *Mater. Des.* **2003**, *24* (3), 197–202.
52. Gomez-Vazquez, O. M.; Correa-Piña, B. A.; Zubieta-Otero, L. F.; Castillo-Paz, A. M.; Londoño-Restrepo, S. M.; Rodriguez-García, M. E. *Ceram. Int.* **2021**, *47* (23), 32775–32785.
53. Yelten-Yilmaz, A.; Yilmaz, S. *Ceram. Int.* **2018**, *44* (8), 9703–9710.
54. Castro, M. A. M.; Portela, T. O.; Correa, G. S.; Oliveira, M. M.; Rangel, J. H. G.; Rodrigues, S. F.; Mercury, J. M. R. *Bol. Soc. Esp. Cerámica Vidr.* **2022**, *61* (1), 35–41.
55. Chen, J.; Liu, J.; Deng, H.; Yao, S.; Wang, Y. *Ceram. Int.* **2020**, *46* (2), 2185–2193.
56. Hassan, M. N.; Mahmoud, M. M.; El-Fattah, A. A.; Kandil, S. *Ceram. Int.* **2016**, *42* (3), 3725–3744.
57. Shi, D.; Tong, H.; Lv, M.; Luo, D.; Wang, P.; Xu, X.; Han, Z. *Environ. Sci. Pollut. Res.* **2021**, *28*

(41), 58189–58205.
58. Eshtiagh-Hosseini, H.; Housaindokht, M. R.; Chahkandi, M. *Mater. Chem. Phys.* **2007**, *106* (2–3), 310–316.
59. Fathi, M. H.; Hanifi, A. *Mater. Lett.* **2007**, *61* (18), 3978–3983.
60. Padmanabhan, S. K.; Balakrishnan, A.; Chu, M.-C.; Lee, Y. J.; Kim, T. N.; Cho, S.-J. *Particuology* **2009**, *7* (6), 466–470.
61. Zhang, J. X.; Guan, R. F.; Zhang, X. P. *J. Alloys Compd.* **2011**, *509* (13), 4643–4648.
62. Munir, M. U.; Salman, S.; Ihsan, A.; Elsaman, T. *Int. J. Nanomedicine* **2022**, *Volume 17*, 1903–1925.
63. Qi, C.; Zhu, Y.-J.; Wu, C.-T.; Sun, T.-W.; Jiang, Y.-Y.; Zhang, Y.-G.; Wu, J.; Chen, F. *RSC Adv.* **2016**, *6* (12), 9686–9692.
64. Utara, S.; Klinkaewnarong, J. *Ceram. Int.* **2015**, *41* (10), 14860–14867.
65. Guo, X.; Yan, H.; Zhao, S.; Li, Z.; Li, Y.; Liang, X. *Adv. Powder Technol.* **2013**, *24* (6), 1034–1038.
66. Javadinejad, H. R.; Ebrahimi-Kahrizsangi, R. *Int. J. Chem. Kinet.* **2021**, *53* (5), 583–595.
67. Javadinejad, H. R.; Ebrahimi-Kahrizsangi, R. *Int. J. Chem. Kinet.* **2021**, *53* (5), 583–595.
68. Pramanik, S.; Agarwal, A. K.; Rai, K. N.; Garg, A. *Ceram. Int.* **2007**, *33* (3), 419–426.
69. Saha Chowdhury, S.; Mishra, D. P.; De, S. *Sep. Purif. Technol.* **2025**, *362*, 131822.
70. Butrin, N.; Rueangchai, N.; Noisong, P.; Sansuk, S. *Mater. Today Commun.* **2024**, *40*, 109615.
71. Yuan, Q.; Wang, P.; Wang, X.; Hu, B.; Wang, C.; Xing, X. *Sci. Total Environ.* **2023**, *865*, 161097.
72. Chen, Y.; Shi, C.; Zhao, B.; Di, D.; Xiao, J.; Chen, G. *J. Alloys Compd.* **2025**, *1022*, 179859.
73. Rout, S.; Yadav, S.; Pansare, L. G.; Shashidhar, R.; Pulhani, V.; Vinod Kumar, A. *Sustain.* **2025**, *5*, 100076.
74. Han, X.; Zhang, Y.; Zheng, C.; Yu, X.; Li, S.; Wei, W. *Chemosphere* **2021**, *264*, 128421.
75. Abukhadra, M. R.; Dardir, F. M.; Shaban, M.; Ahmed, E. A.; Soliman, M. F. *Ecotoxicol. Environ. Saf.* **2018**, *157*, 358–368.
76. Ma, J.; Xia, M.; Zhu, S.; Wang, F. *J. Hazard. Mater.* **2020**, *400*, 123143.
77. Xu, Y.; Tang, H.; Wu, P.; Chen, M.; Shang, Z.; Wu, J.; Zhu, N. *Chemosphere* **2023**, *321*, 138123.
78. Ain, Q. U.; Zhang, H.; Yaseen, M.; Rasheed, U.; Liu, K.; Subhan, S.; Tong, Z. *J. Clean. Prod.* **2020**, *247*, 119088.
79. Butrin, N.; Rueangchai, N.; Noisong, P.; Sansuk, S. *Mater. Today Commun.* **2024**, *40*, 109615.
80. Billah, R. E. K.; Abdellaoui, Y.; Anfar, Z.; Giácoman-Vallejos, G.; Agunaou, M.; Soufiane, A. *Water. Air. Soil Pollut.* **2020**, *231* (4), 163.
81. Fadila, C. R.; Othman, M. H. D.; N.J., I.; Takagi, R.; Yoshioka, T.; Khongnakorn, W.; Rahman, M. A.; Jaafar, J.; Borhamdin, S.; Ismail, A. F. *Mater. Today Proc.* **2023**, S2214785323005412.
82. Sasirekha, R.; Vijayakumar, S.; Pazhanisamy, P.; Joseph, J. J.; Gomathi, T. *Mater. Today Commun.* **2023**, *35*, 106339.
83. Sayed, I. R.; Farhan, A. M.; AlHammadi, A. A.; El-Sayed, M. I.; Abd El-Gaied, I. M.; El-Sherbeeny, A. M.; Al Zoubi, W.; Ko, Y. G.; Abukhadra, M. R. *J. Mol. Liq.* **2022**, *360*, 119527.
84. El Kaim Billah, R.; Ayouch, I.; Abdellaoui, Y.; Kassab, Z.; Khan, M. A.; Agunaou, M.; Soufiane, A.; Otero, M.; Jeon, B.-H. *Polymers* **2023**, *15* (6), 1524.
85. Gibert, O.; Valderrama, C.; Martínez, M. M.; Darbra, R. M.; Moncunill, J. O.; Martí, V. *Water* **2021**, *13* (11), 1493.
86. El KaimBillah, R.; Islam, Md. A.; Agunaou, M.; Soufiane, A. *Arab. J. Geosci.* **2021**, *14* (12), 1134.
87. Kaim Billah, R. E.; . Elyamani, Y.; . Rakhila, Y.; . Agunaou, M.; . Soufiane, A. *Rasayan J. Chem.* **2019**, *12* (1), 347–354.
88. Szcześ, A.; Hołysz, L.; Chibowski, E. *Adv. Colloid Interface Sci.* **2017**, *249*, 321–330.
89. Zhang, Z.; Wang, X.; Wang, H.; Zhao, J. *Chem. Eng. J.* **2018**, *344*, 53–61.
90. Miyah, Y.; El Messaoudi, N.; Benjelloun, M.; Acikbas, Y.; Şenol, Z. M.; Ciğeroğlu, Z.; Lopez-Maldonado, E. A. *Chemosphere* **2024**, *358*, 142236.